AD-A244 546

ATION PAGE

Form Approved
OMB No. 0704-0188

average 1 hour per response, including the time for reviewing instructions, searching existing data sources,
ng the collection of information Send comments regarding this burden estimate or any other aspect of this
to Washington Headquarters Services, Directorate for Information Operations and Reports, 1215 Jefferson
Y Management and Budget, Paperwork Reduction Project (0704-0188), Washington, DC 20503.

	ATE June 1991	**3. REPORT TYPE AND DATES COVERED** Conference Paper Reprint

4. TITLE AND SUBTITLE
Laser Velocimetry Measurements of Oscillating Airfoil
Dynamic Stall Flow Field

5. FUNDING NUMBERS

ARO MIPR 114-91

6. AUTHOR(S)
M. S. Chandrasekhara and S. Ahmed

DTIC
ELECTE
JAN 21 1992
S D

7. PERFORMING ORGANIZATION NAME(S) AND ADDRESS(ES)
Naval Postgraduate School
Navy-NASA Joint Institute of Aeronautics
Monterey, CA 93943

8. PERFORMING ORGANIZATION REPORT NUMBER
--

9. SPONSORING/MONITORING AGENCY NAME(S) AND ADDRESS(ES)
U. S. Army Research Office
P. O. Box 12211
Research Triangle Park, NC 27709-2211

10. SPONSORING/MONITORING AGENCY REPORT NUMBER
ARO 27894.6-EG

11. SUPPLEMENTARY NOTES AIAA Paper No. 91-1799
The view, opinions and/or findings contained in this report are those of the
author(s) and should not be construed as an official Department of the Army
position, policy, or decision, unless so designated by other documentation.

12a. DISTRIBUTION/AVAILABILITY STATEMENT

Approved for public release; distribution unlimited.

12b. DISTRIBUTION CODE

92-00954

13. ABSTRACT (Maximum 200 words)

Ensemble averaged two components velocity measurements over an airfoil experiencing
oscillatory dynamic stall under compressibility conditions were obtained. The
measurements show the formation of a separation bubble over the airfoil that persists
till angles of attack close to when the dynamic stall vortex forms and convects. The
fluid attains mean velocities as large as 1.6 times the free stream velocity (U_∞)
with instantaneous values of $1.8 U_\infty$. The airfoil motion induces these large velocities
in regions that are far removed from its surface. Also, depending upon the behavior
of the separation bubble, the wall jet profiles near the leading edge region could
become wake like over the airfoil in a cycle at different phase angles. Vorticity
contours indicate that the levels around the leading edge continuously increase till
the vortex begins to convect. Some of the measurements difficulties, especially,
particle behavior are discussed as well.

14. SUBJECT TERMS
LV measurement, dynamic stall, unsteady random data alquisition

15. NUMBER OF PAGES
12

16. PRICE CODE
--

17. SECURITY CLASSIFICATION OF REPORT	**18. SECURITY CLASSIFICATION OF THIS PAGE**	**19. SECURITY CLASSIFICATION OF ABSTRACT**	**20. LIMITATION OF ABSTRACT**
UNCLASSIFIED	UNCLASSIFIED	UNCLASSIFIED	UL

NSN 7540-01-280-5500

Standard Form 298 (Rev 2-89)

92 1 21 046

AIAA-91-1799

Laser Velocimetry Measurements of Oscillating Airfoil Dynamic Stall Flow Field

M. S. Chandrasekhara, Naval Postgraduate
School and Navy-NASA Joint Institute
of Aeronautics, Monterey, CA;
S. Ahmed, MCAT Institute, San Jose, CA.

Accesion For		
NTIS CRA&I		☑
DTIC TAB		☐
Unannounced		☐
Justification		
By		
Distribution		
Availability		
Dist	Avail and / or Special	
A-1		

AIAA 22nd Fluid Dynamics, Plasma Dynamics & Lasers Conference
June 24-26, 1991 / Honolulu, Hawaii

Laser Velocimetry Measurements of Oscillating Airfoil Dynamic Stall Flow Field

By

M.S.Chandrasekhara[1]
Navy-NASA Joint Institute of Aeronautics
and Fluid Mechanics Laboratory, NASA Ames Research Center
Department of Aeronautics and Astronautics
Naval Postgraduate School, Monterey, CA 93943

and

S.Ahmed[2]
MCAT Institute, San Jose, CA 95127

Abstract

Ensemble averaged two component velocity measurements over an airfoil experiencing oscillatory dynamic stall under compressibility conditions were obtained. The measurements show the formation of a separation bubble over the airfoil that persists till angles of attack close to when the dynamic stall vortex forms and convects. The fluid attains mean velocities as large as 1.6 times the free stream velocity(U_∞) with instantaneous values of $1.8U_\infty$. The airfoil motion induces these large velocities in regions that are far removed from its surface. Also, depending upon the behavior of the separation bubble, the *wall jet* profiles near the leading edge region could become *wake like* over the airfoil in a cycle at different phase angles. Vorticity contours indicate that the levels around the leading edge continuously increase till the vortex begins to convect. Some of the measurement difficulties, especially, particle behavior are discussed as well.

Nomenclature

c	airfoil chord
f	frequency of oscillation, Hz
k	reduced frequency $= \frac{\pi f c}{U_\infty}$
M	free stream Mach number
U,V	velocity components in the x and y directions
U_∞	free stream velocity
x,y	chordwise and vertical distance
α	angle of attack
α_0	mean angle of attack
α_m	amplitude of oscillation
ϕ	phase angle of oscillation
ω	circular frequency, radians/sec

---

1 *Assistant Director and Adjunct Research Professor; Associate Fellow, AIAA. Mailing Address: M.S. 260-1. NASA Ames Research Center, Moffett Field, CA 94035*
2 *Research Scientist; Member AIAA. On Leave from National Aeronautical Laboratory, Bangalore, India*

1. Introduction

The phenomenon of dynamic stall is an important case of forced unsteady separated flow and is of great importance to both helicopters and fixed wing aircraft. Dynamic stall relates to production of lift at angles of attack higher than the static stall angle by rapidly pitching an airfoil - a situation routinely encountered in helicopter blade motion. The major benefit of dynamic stall, namely, enhanced lift has remained unutilized because of the detrimental effects of the associated pitching moment fluctuations due to the convection of the dynamic stall vortex over the airfoil upper surface. A solution to the problem lies in controlling the process of flow separation and management of vorticity produced by the rapid pitching process. However, to accomplish this, a thorough understanding of the physics of the flow over the airfoil, especially around the leading edge is needed. The process of dynamic stall is very complex and Carr[1] provides a comprehensive review of the problem. The importance of compressibility, even at a low free stream Mach number of 0.2 has been established by the earlier work of McCroskey[2]. Harper and Flanigan[3] found that the benefits of dynamic stall, namely the production of enhanced lift, were negated by compressibility. Recently, Chandrasekhara and Carr[4], Chandrasekhara and Brydges[5]. Chandrasekhara et al[6] have studied the global dynamic stall flow field by flow visualization, and found that compressibility effects set in at M = 0.3, and that the flow field is significantly affected, but the dynamic lift is still generated. Much of the earlier work referred to above is either globally qualitative or locally quantitative and limited to the

surface. About the only quantitative documentation of the flow field that exists was obtained by DeRuyck et al[7] at a very low flow velocity (O (10 m/s)). The low speed of the experiment and the use of hot wires in grossly separated flows severely limits the validity and usefulness of the data.

The dynamic stall flow field is a complicated combination of a multitude of fluid dynamic effects such as tremendous acceleration around the leading edge, formation of strong suction peaks, development of the local boundary layer under the strongly adverse pressure gradient following such acceleration, transition of the laminar boundary layer, separation of the boundary layer and its reattachment resulting in a separation bubble, its subsequent growth and eventual bursting just before the formation of the dynamic stall vortex, formation of shock(s) and the induced separation due to it, addition of large amounts of coherent vorticity into the flow and its coalescence into the dynamic stall vortex and so on. The interaction between the various phenomena and the trailing edge separated flow that propagates towards the leading edge only add to the flow complexity. For proper control schemes to be devised to manage this flow, it is obvious that a careful and thorough study of the basic fluid flow physics is needed to isolate the individual effects and the role of various parameters. A survey of the computational studies shows that Grohsmeyer et al[8], Ekaterinaris[9], Courier and Fung[10] have begun to address some of the above mentioned issues. However, there is no experimental data available for the comparison and validation of the computational results.

The present work is aimed at quantifying the velocity field with the hope that some progress can be made in understanding the flow physics, with which ideas of dynamic stall flow control can be developed, while at the same time the data base generated will serve to verify computational results and also enable development of new codes that incorporate appropriate flow physics.

2. Description of Facility

The experiments were conducted in the in-draft wind tunnel of the Fluid Mechanics Laboratory(FML) at NASA Ames Research Center (ARC). It is one of the ongoing dynamic stall research projects in the Navy-NASA Joint Institute of Aeronautcis between the Naval Postgraduate School and NASA ARC.

The details of the FML in-draft wind tunnel are given in Carr and Chandrasekhara[11]. The facility is one of a complex of four in-draft wind tunnels connected to a $108m^3/sec$ (240,000 CFM), 9,000 hp evacuation compressor. The test section size is 25.4cm X 35cm X 100cm The flow in the tunnel is controlled by a variable cross section downstream diffuser. Its throat is always kept choked so that no disturbances can propagate upstream into the test section from the other tunnels or the compressor.

A unique mechansim was designed and built to produce the oscillatory motion of the airfoil. It is described in Ref. 11 The drive system is located on top of the test section. The test section windows are connected to the drive and the sinusoidal movement of

the windows results in an identical movement of the airfoil which is supported by the windows. The airfoil is supported by pins push fitted between two 2.54cm thick optical quality glass windows. The airfoil supports are unique in that the pins carry the entire load. The pins are smaller than the local airfoil thickness and hence provide complete optical access to the airfoil surface. This makes detailed flow studies possible even at the surface.

The oscillating drive was designed to meet the following specifications:

$$\alpha = \alpha_0 + \alpha_m sin2\pi ft = \alpha_0 + \alpha_m sin\omega t$$

$$0 \leq \alpha_0 \leq 15^0$$

$$2^0 \leq \alpha_m \leq 10^0$$

$$0 \leq f \leq 100Hz$$

$$0 \leq M_\infty \leq 0.5$$

$$200,000 \leq Re \leq 10^6$$

$$\text{airfoil chord} = 7.62cm$$

The flow conditions correspond to a helicopter in forward flight and the Reynolds number corresponds to that of a $\frac{1}{7}$th scale model rotor, whose test results are directly applicable to a helicopter rotor. The in-draft wind tunnel and the unsteady drive system is known as the *Compressible Dynamic Stall Facility (CDSF)*. Fig. 1 provides a schematic of the facility and its instrumentation.

3. Instrumentation and Measurement Technique

A. Phase Locking Instrumentation

The CDSF is instrumented with 3 digital encoders. Of these, one is an absolute position encoder providing 3600 counts per revolution and is used for the mean angle of attack information. The other two are incremental position encoders with a resolution of 800 counts per revolution. One of the incremental encoders is used for obtaining the frequency/phase angle information. The other could be used for the instantaneous angle of attack. But, for the series of experiments being reported, it was not used.

A two color, two component frequency shifted TSI LDV system was used to obtain the measurements. Traversing was accomplished by directing the 4 beams of the system by mirrors on to a 352 mm focal length lens mounted on a computer controlled traverse. The scattered light was collected 15 degrees off-axis from direct forward scatter, this provided a reduced probe volume length and thus, improved the measurement resolution. The receiving optics were on a different traverse mechanism, but this was driven as a slave traverse to that on the transmitting side, and the two sides were kept aligned throughout. Two TSI 1990 series counters were used to process the individual photomultiplier tube signals.

Unsteady flow studies using LDV require phase locking circuitry that are capable of handling the random nature of the LDV data. Since the LDV data

rate is dependent on particle arrival rate, which is in general random and a function of the local flow, there is a need to read the instantaneous phase angle each time an LDV data sample is validated. This requires latching circuits to freeze the continuous encoder data based on an event in the flow. In the present experiments, this event was specified to be the occurence of coincident LDV data i.e. simultaneous Doppler signals in both the U and V components. The coincidence window width was chosen to be $50\mu sec$. The LDV data was input to a NASA LDV multiplexer, to which the encoder outputs processed by the counting circuitry were also connected. The coincidence detection pulse (i.e. the data ready pulse) from the multiplexer was used to freeze the encoder data at that instant, until all the data was completely transferred to a microVAX II computer in the DMA mode. As soon as this was accomplished, the latches were released for fresh data. In view of the high oscillation frequencies encountered, changes in the instantaneous angle of attack would occur in the time it takes to freeze the encoders. This along with the general paucity of the LDV data and the time it takes to transfer it to the computer required high speed latches to be used. Fig. 2 presents a schematic of the method followed. This inverse method of data collection is considered superior to specifying the phase angle and waiting for a certain sample size to be collected.

B. The Technique

As mentioned above, velocity data was acquired each time both components were available simultaneously. Concurrently, the various encoders were also read. In general, 10,000 coincident samples of each of U and V velocity components were obtained along with the encoder information for each sample. The process was computer controlled by an extensive software package that was specially developed for the purpose. The software capabilities include checks for detecting the oscillating drive frequency variations beyond a pre-set tolerance, sorting the data into bins and plotting histograms and velocity *vs.* phase angle distributions. At any stage when the data appeared not to pass the standard tests of data validation, (for example a widely scattered histogram), the entire data set was rejected and new data was acquired. The data was sorted into 36 bins corresponding to different phase angles in a $\pm 5^0$ range. If the distributions indicated any irregularities, then the data was rejected and the experiment repeated. Since such irregularities could be due to improper setting of the gains and the filters (it should be noted that the flow has a very large dynamic range in this experiment through an oscillation cycle), the electronic components were very carefully set and the setting maintained. Since this often resulted in reduced data rates, the collection of samples took several minutes at each point, (as much as 30 min. at some locations). However, this was preferred to any other means of increasing the data rate because of the truly unsteady nature of the flow and the large dynamic range dictated by the fluid dynamics of the problem. This procedure was repeated at each measurement location. Typically, a vertical velocity traverse above the airfoil surface consisted of 40

stations, acquiring 10,000 samples per channel along with the three encoder outputs, namely, mean angle of attack, phase angle and frequency of oscillation, per sample - all measurements were stored on disk and archived on tape.

During the analysis stage of the experiment, the raw data files were processed by another package by sorting into 120 bins at a resolution of $\pm 1.5^0$ and the plots displayed on the screen. At this stage, a minimum number of samples could be set depending upon the demands of statistical stationarity. The results presented here were obtained by stipulating that each phase angle bin contained at least 50 samples. When ever the required number of samples was not present in any bin, that bin was said to contain a 'hole'. A monotonic spline curve fit was then used to interpolate the data to 'fill the hole' between valid data bins. This method worked successfully over most phase angles of interest for the problem.

Data was acquired in a rectangular x-y grid, with x and y measured from the leading edge of the airfoil when its angle of attack was zero degrees.

C. Seeding

The flow was seeded with 1 μm polystyrene latex particles(PSL) suspended in alchohol and dispersed by the TSI 9306 six-jet atomiser. The particles were injected from slightly behind the indraft tunnel inlet continuously and arrived at the probe volume after travelling a distance of over 3 meters, by which time the alchohol had evaporated and only the PSL remained. The location of the injector was adjusted to suit the streamline pattern at different measurement points.

D. Experimental Conditions

The flow Mach number was set to 0.3. The oscillation frequency was 21.6 Hz which corresponded to a reduced frequency of 0.05. The airfoil was NACA 0012 airfoil, oscillating about the 25% chord point, with its angle of attack varying as

$$\alpha = 10^0 - 10^0 sin\omega t$$

Thus, phase angle of 0^0 corresponded to $\alpha = 10^0$, 90^0 to $\alpha = 0^0$ on its downstroke, 180^0 to $\alpha = 10^0$ on the upstroke and 270^0 to the maximum angle of attack of 20^0. The LDV probe volume was traversed in the range $-0.25 \leq x/c \leq 0.75$, $0.0 \leq y/c \leq 0.67$. The resolution was 6.25mm in the x direction and 1.25mm in the y direction.

3. Results and Discussion

A summary of the data to be presented is shown in Fig 3. Following a measurement of the two dimensionality of the flow along a spanwise line at location B, time-histories of streamwise velocity at positions A,B,C,D are compared and contrasted. The next data set will concentrate on details of the separation region enclosed in the box E. The final set of measurements will examine the velocity and vorticity fields in the larger region denoted by the box F

A. Two-Dimensionality Surveys

The tunnel flow two dimensionality was studied with the airfoil oscillating for M = 0.3, k = 0.05, at location x/c = 0.0 (i.e. nominally the leading edge) and y/c = 0.167 for several spanwise locations. Distributions of the normalized streamwise velocity component are shown in Fig. 4 at five spanwise locations on an offset scale. As can be seen, the curves are parallel everywhere through the oscillation cycle to within 5%, except in the range $216^0 \le \phi \le 320^0$. Earlier schlieren flow visualization experiments by Chandrasekhara and Carr[4] have shown that for the experimental conditions of this graph, deep dynamic stall occurs at $\alpha = 15.9^0$ corresponding to $\phi = 216^0$ when the dynamic stall vortex is shed. The upstream effects of the large scale flow separation and the large vertical flow scales are responsible for the differences seen after stall. However, the flow can be treated as essentially two-dimensional over the phase angle range of interest through the central two-thirds of the test section. Measurements beyond these stations were either difficult due to seeding problems or the LDV probe volume was not 'visible' to the receiving optics because of the off-axis forward scatter arrangement used. All further measurements were hence restricted to the mid-span plane.

B. Selected Distribution of $\frac{U}{U_\infty}$ vs Phase Angle

Fig. 5 presents the phase variation of the normalized U and V velocity components at selected locations in the flow field. Dramatic variations are to be expected in a complex flow such as this and hence, the following discussion.

In Fig. 5a, at x/c = -0.25, y/c = 0.583, a location upstream of the airfoil leading edge, the flow almost follows the sinusoidal motion imposed by the oscillating airfoil. The most noteworthy feature at this station is that the peak velocity is $1.15U_\infty$ and occurs at a phase angle of about 216^0, which corresponds to the dynamic stall angle as already stated. Beyond this phase angle, the separated flow causes the velocity to drop as the streamlines are decelerated when the airfoil continues to pitch up and the flow gets blocked by the high angle of attack of the airfoil. In fact, the effects remain until the flow reattaches at around a phase angle of $\approx 330^0$. Only after the flow is fully reestablished, does the velocity increase again. The V velocity distribution in Fig. 5b shows a velocity of about 6-8% of the free stream value at $\phi = 0^0$, i.e. at $\alpha = 10^0$, which drops to about 2-3% at $\phi = 90^0$, $\alpha = 0^0$ and starts to increase as the airfoil pitches up, reaching a peak value of $0.12U_\infty$ at $\phi = 216^0$. Once again, the value remains high as the streamlines are deflected upward while being slowed down due to massive flow separation until reattachment[4] becomes complete.

At x/c = 0.0, (the leading edge at $\alpha = 0^0$), the fluid experiences much more dramatic accelerations and decelerations through the cycle. For example, during the pitch down cycle of the airfoil $0 \le \phi \le 90^0$, the fluid velocity decreases from $1.2U_\infty$ to about $0.9U_\infty$. As the airfoil pitches up, the fluid around the leading edge is drawn with it and is imparted the accelerations of the moving surface and eventually by $\phi = 216^0$, it has attained a velocity of $1.3U_\infty$. As deep dynamic stall occurs, the velocity drops significantly to $0.85U_\infty$ and remains low till reattachment. The corresponding V velocities have reached values as high as 30% of the free stream value at $\phi = 0^0, \alpha = 10^0$, but decrease to about $0.15U_\infty$ at $\phi = 90^0, \alpha = 0^0$, and increase to nearly $0.6U_\infty$ at $\phi = 216^0$. During the deep dynamic stall phase of the motion, the V component of velocity remains high.

A very interesting case of the U velocity field is seen in Fig. 5a for x/c = 0.083, y/c = 0.067. (At this location, no samples could be found for $0 \le \phi \le 30^0$ and the airfoil blocks the beams for $190^0 < \phi < 360^0$. The non zero values shown are an artifact of the data processing routine for such cases.) As the airfoil angle of attack decreases, the velocity drops from $1.35U_\infty$ (at $\phi = 30^0, \alpha = 5^0$) to $1.05U_\infty$ at $\phi = 90^0, \alpha = 0^0$ and increases as the upward motion of the airfoil begins. At $\phi \approx 160^0$, ($\alpha = 6^0$) the maximum velocity of $1.45U_\infty$ in the cycle is reached and suddenly, over a very short phase angle range, the velocity drops by 45% to $0.8U_\infty$ and picks up slightly, before the beams are blocked by the moving airfoil. The significance of the drop is that the probe volume is penetrated by the separation bubble on the airfoil surface which moves with the airfoil and grows with increasing angle of attack. It is worth mentioning here that a bubble was also detected at this phase angle for this flow conditions in a separate study using interferometry[12]. Inside the bubble, the velocities are smaller than around it. The V velocity component remains high at $0.2U_\infty$ for most part where measurements could be obtained, but shows a drop through the bubble. The measurement point is estimated to be about 1-2% chord above the airfoil surface at this phase angle, and measurements closer could not be obtained due to the airfoil blocking the laser beams.

At x/c = 0.75 and y/c = 0.133, a point downstream of the point of oscillation, the velocity through the first half of the oscillation cycle are lower than the free stream value. But, as before, it increases during the upward motion of the airfoil until the deep dynamic stall phase of the cycle. Interestingly, the magnitude is $\approx 1.1U_\infty$ at this point and it does not drop during this phase at all. The V component is negative everywhere with a maximum of $-0.2U_\infty$. The streamlines are curving towards the airfoil surface at this location throughout the cycle and the local flow is three dimensional and turbulent during deep stall.

The above discussion provides a glimpse into the complexity of the flow field and the variety of possibilities encountered in large amplitude dynamic stall flow.

C. Velocity vs Phase at Different Vertical Locations: Measurements in the Separation Bubble

Fig. 6 shows the distribution of the U and V velocities with phase at x/c = 0.083. At this particular location, a separation bubble was present. Thus, the distributions in Fig. 6a show some very interesting

4

features. For example, at $y/c = 0.067$, at $\phi = 160^0$, the velocity drops as already discussed in Sec. B above. It should be noted that in unsteady flows, separation does not necessarily imply reverse flows and thus, over most of the bubble, only lower than free stream velocities were encountered. Reverse flows are expected to be present only very close to the wall and as stated earlier, measurement access down to the wall was not possible due to the beam configuration used. At the higher y/c locations, the phase angles at which the dip in velocity occurs is progressively higher due to the shape of the separation bubble and the airfoil motion till $y/c = 0.150$. (The data for $y/c = 0.1$ showed holes for $180^0 \leq 345^0$) Beyond this point, the distributions are nearly parallel, indicating that these points are clearly outside the bubble. From this data and the airfoil profile at $\phi = 200^0$, it appears that the maximum bubble height is 3-4% chord above the airfoil surface.

A look at the V component of velocity shows a nearly constant velocity through the bubble, for $y/c = 0.067$, till $\phi = 186^0$ where a decrease is observed. For $y/c = 0.117$, a gradual increase occurs through the bubble. For $y/c = 0.133$ and 0.150, at $\phi \approx 200^0$, $\alpha = 13.4^0$, an abrupt increase in the V velocity develops. It is believed that this change is due to the bubble breaking up at $\phi \approx 200^0$. When this happens, the streamlines around it are pushed outward and thus, an increase is seen at higher locations as well. As the dynamic stall angle is approached, the outer deflection of the streamlines is even more pronounced and this translates to even higher V velocities.

Similar trends were also measured at $x/c = 0.167$, but the bubble was found only at $y/c = 0.083$. Very closely spaced surveys by Chandrasekhara and VanDyken[13] confirmed this to be the case and also showed that the extent of the bubble is approximately $0.15c$ covering the range $0.017 \leq x/c \leq 0.167$.

It is interesting to compare the picture of the development of the bubble with that obtained using point diffraction interferometry (PDI) (Carr et al[12]). The interferometry results show that the bubble forms at nearly the same angle as was seen in the LDV studies and grows till it breaks up. The PDI images show that the dynamic stall vortex forms during the breaking up process and the constant density contours develop appropriate curvature subsequently on its front side. On the back side, however, the flow is very turbulent and thus, only a few density contours could be seen The L .V data of Chandrasekhara and VanDyken[13] shows that the velocities rise when the bubble breaks at around $\phi = 200^0$, indicating a fair degree of mixing between the ambient fluid and the bubble fluid. Thus the spanwise averaged instantaneous flow measurements and the long time averaged point measurements agree reasonably well. Finer details of the flow need more sophisticated methods of extracting the flow information.

D. Velocity Profiles at Different x/c Locations

The velocity profiles at different phase angles are shown in Fig 7a for $x/c = 0.0$ and in Fig. 7b for $x/c =$ 0.083 at selected phase angles ranging from before the bubble formation to after occurence of deep dynamic stall. It is clear that the range of the velocities is much larger at $x/c = 0.083$ than at $x/c = 0.0$. For example, at $y/c = 0.1$, the maximum velocity is $1.6U_\infty$ at $\phi = 150^0$ and $1.64U_\infty$ at $\phi = 171^0$. The corresponding values for $x/c = 0.0$ are $1.56U_\infty$ and $1.52U_\infty$ respectively. Regardless, it is much higher than the free stream value and is due to two factors: (1) airfoil angle of attack and (2) the airfoil motion. Ericsson[14] has referred to the latter as the 'moving wall effect' wherein the fluid in the boundary layer is energized by the rapidly moving airfoil, thus acquires the ability to resist the adverse pressure gradient and hence, separation is delayed. A quantitative documentation of this effect was hitherto not available. The present results show that the 'leading edge jet effect' resulting in the *wall jet* like velocity distribution actually is felt considerably into the outer flow and is not just confined to near the wall. Also, it extends sufficiently downstream over the airfoil. Despite the fact that the velocities decrease in the separation bubble, the velocity immediately outside of it is extremely large, about $1.6U_\infty$. The acceleration is being felt from very low angles of attack, in fact, even at $\alpha < 5^0$ and thus, is clearly due to the moving wall because, at low angles of attack, the velocity at the leading edge is not very large and also, the dynamic stall vortex has not yet formed and thus, the flow is still attached and follows the airfoil profile. It is also to be noted that the velocity of the airfoil leading edge is a maximum of $\approx 3\%$ of the free stream value, but still the effects of the airfoil pitching are very strong. This implies that the degree of unsteadiness, if measured as a ratio of the leading edge velocity to the free stream velocity, shows a large effect even at very low values.

As the airfoil angle of attack increases beyond the static stall angle (12.4^0), the fluid velocity closer to the surface decreases as can be seen in Fig. 7a and 7b. Also, in Fig. 7b, a *wake like* profile emerges for $\phi > 198^0$. This change is believed to be due to the opening out of the bubble and the gushing of the fluid surrounding it immediately following the event. Further, the location of the maximum defect moves closer to the surface as the angle of attack increases. Typical velocity defects measured were about $0.2U_\infty$.

Fig. 7c shows the velocity profiles at $x/c = 0.583$. At low phase angles, $\phi \leq 200^0$, the profiles are the same as the local boundary layer as at this location, it is about 4-5% chord thick depending upon the angle of attack. Thus, a few measurement points could be obtained. At larger phase angles, at this location, the effect of the dynamic stall vortex is felt strongly. The vortex increases the velocity in the outer flow and decreases in the inner flow. It appears that the flow is very turbulent and unsteady within the vortex. Thus, measurements during its passage through the measurement voulme, show the effects as wiggles in the velocity profiles The effect propagates to larger y/c locations as the angle of attack increases and the vortex grows in size. No negative U velocities were measured anywhere in the measurement grid and thus, the vortex as such could not be identified. But, the large scale distortions in the profiles are indicative of the passage of the vortex. (see also Sec. G)

5

E. Global Distributions of Absolute Velocity

Fig. 8 shows the absolute velocity vectors plotted at the local flow angle in the flow field. Fig. 8a is drawn for $\phi = 90^0$, or $\alpha = 0^0$ and indicates that even though the airfoil is at zero degrees angle of attack, the velocities over the airfoil exceed the free stream slightly. The vertical velocities were found to be non zero for this condition even in the outer flow, a clear indication of the presence of hysterisis effects of oscillation. Closer to the airfoil leading edge, in addition, the fluid still has to negotiate the curvature and hence, a slight positive (upward) velocity is measured. The figure shows that the streamlines are nearly horizontal, except around the leading edge.

Fig. 8b shows the absolute veloity field at $\phi = 201^0, \alpha = 13.58^0$. The rapid flow accelerations are clearly seen well into the outer flow in it, as also, the wake like distributions discussed above at $x/c = 0.083$. The slowing down of the flow is also evident near the airfoil surface at larger x/c locations. From the orientation of the velocity vectors it can be inferred that the vertical velocities around the leading edge are large. In fact, the V velocity could reach a value of $0.5U_\infty$. The effects of the airfoil motion are seen once again at very large ($0.5c$) y/c values. The effects are the strongest at both upstream locations ($x/c = -0.083$ and $x/c = 0.0$) and at $x/c = 0.083$. By $x/c = 0.25$, the fluid is turning inward and as the fluid moves downstream, it turns even more. The schlieren studies of Chandrsaekhara and Carr[4] have shown that at this angle of attack, the dynamic stall vortex has just formed, and the measured behavior is consistent with that study. In general, the outer flow is only slightly turning, but the inner flow streamlines are curving strongly upward around the leading edge, but by $x/c = 0.25$, the flow is pointing downward. Also, the decreasing velocities closer to the surface at larger x/c distances are also clearly seen.

At $\phi = 216^0$, the airfoil is at the dynamic stall angle and the velocity profiles exhibit large changes at some locations, and the dynamic range is also large. Yet, no negative velocities are seen. Even in the region enveloped by the leading edge shear layer and the dynamic stall vortex, large velocities are seen. One of the reasons for this is that the reverse flow region is expected to be only about 2-3% chord thick at best and the negative velocities in it are likely to be small. Since the vortex is being convected at $0.3U_\infty$[4], it is unlikely that large reverse flow velocities will be encountered. Once again, the vectors show that at this angle of attack, the leading edge flow has been pushed away from the airfoil, an effect felt over wide distances.

Fig. 9a presents the contours of the absolute velocity for some of the above cases. It is seen that even at $\alpha = 0^0$, the velocity range is from 0.88 - $1.1U_\infty$. At $\alpha = 8.95^0$, Fig. 9b, the contour lines (12) show a maximum velocity of $1.45U_\infty$. It is found in a pocket of fluid above the airfoil surface. Between this fluid and the airfoil, lower velocities could be found. It should be recalled here that a separation bubble was detected here. In Fig. 9c, as the angle of attack increases to 14.07^0, the peak velocity reaches $1.55U_\infty$, but the fluid is at $0.1c$ above the surface, at $x/c =$

0.08 - 0.1. Also, the leading edge wall jet effect is seen clearly. Further, following contour line 15, the wake like profile could also be found between $x/c = 0.16$ - 0.2. Regions of low velocity are developing beyond $x/c = 0.3$, but near the leading edge, at $y/c = 0.05$, the velocity is still $1.15U_\infty$. This figure resembles the interferogram obtained for the same conditions(Carr et al[14]). Finally, in Fig. 9d, at $\phi = 216^0$, it is interesting to note that several pockets of high fluid velocity ($1.4U_\infty$, contour line 19) form in the shear layer extending to $x/c = 0.45$ and $y/c = 0.25$. The velocities around the leading edge are still large, even under this condition. But, the flow towards the trailing edge is moving very slowly at $0.5U_\infty$. Significant structure can also be seen in the flow.

F. Vorticity Distributions

The z-component of vorticity (normalized by $\frac{c}{U_\infty}$) was calculated from the measured U and V components of velocities by first fitting a cubic spline curve to the data and interpolating the velocities in a grid at a resolution of 1.25mm - using a second order central differencing scheme. Thus, the noise level in the distributions is expected to be high at about 20% of the local maximum vorticity values (in both the positive and negative quantities). The following discussion about the vorticity field should be still valid, especially before the dynamic stall vortex begins to convect (see also Sec. G), because no discontinuities such as shocks were encountered within the measurement grid. The picture of the flow field thus is also quantitatively valid up to the point where the particles were able to follow the flow adequately.

Fig. 10a shows that at $\phi = 171^0$ ($\alpha = 8.44^0$), a region of clockwise vorticity has developed over the airfoil, just around the location of the separation bubble, with a peak vorticity of -8 units in it. A region of counter clockwise vorticity could also be found above it, but the peak vorticity in it is only about 5 units. As the airfoil reaches an angle of attack of 10 degrees, Fig. 10b, the clockwise vorticity has increased to -11 units, whereas the anticlockwise vorticity is still at 5 units. The extent of the vortical region has grown to about 25%chord in both the x and y directions. As the airfoil pitches to higher angles of attack, the vorticity should steadily increase until stall occurs. Fig. 10c shows that at $\phi = 198^0$, this is the case as the clockwise vorticity has doubled to -22 units, but the anticlockwise vorticity has only increased to about 10 units. Earlier experiments[4] have shown that the vortex begins to convect at around this phase angle. The separation bubble also bursts around the same angle of attack. Thus, a combined effect is felt by the airfoil, which should be seen in its vorticity field. By the time dynamic stall occurs, at $\alpha = 15.9^0$, the clockwise vorticity has increased to about -31 units, but the counter clockwise vorticity is still small at 12 units. Beyond this angle, the vortex is shed and so the total circulation over the airfoil should decrease.

Fig. 11 presents a plot of the 'net circulation' over the measurement grid. The computed vorticities were integrated by including only the values that were above the noise level (arbitrarily chosen to be 25% of the local maximum) for vorticity of both signs

6

to get the circulation. This graph has the same limitations as the vorticity field. However, some clear trends are evident and hence, the results are presented. It can be seen that the 'net circulation' monotonically increases till phase angle of 200^0 is reached when the vortex convection starts. Nearly a 10 fold increase was obtained in the upstroke of the airfoil from $\alpha = 5^0$ to $\alpha = 13^0$. The changes seen between $\phi = 200^0 - 216^0$ are believed to be due to the inability of the LDV seed particles to follow the rapid changes in the flow. However, near the dynamic stall angle, a slowly decreasing trend is observed. Some of the discrepancies noted here are due to the fact that the entire upper surface data has not yet been obtained and also due to the approximations made in reaching this stage.

G. Discussions of the Measurement Challenges

The measurements reported in this paper were obtained after partially solving some of the formidable challenges posed by the flow, flow geometry and the measurement technique. It is worth stating before proceeding further that the mean velocity measurements repeat to within 5% at any given station over most of the oscillation cycle. The unsteady nature of the flow and the large amplitude of oscillation of the experiment required acquiring a very large amount of data over the cycle to realize low uncertainty levels. The 10,000 samples/per point collected in this experiment ensures that this can be achieved, but a better accuracy could be obtained if a much larger number of samples, say 50,000 could be obtained. However, the extent of the flow field surveyed would mean an experiment that runs for several months with the airfoil oscillating, leading to other difficulties. This would still not guarantee that adequate number of samples will be found in each phase angle bin of interest from 180^0 to 216^0 due to the randomness of the particle arrival rate in the probe volume. The problems of the particle arrival in the measurement volume and particle lag are especially accute after the vortex forms and convects because the particles have to follow the rapid accelerations experienced by the flow in the shear layer that envelops the vortex. Given that the frequency of oscillation is 21.6 Hz and hence that the vortex is shed about once every 50 milliseconds, this is a challenge. In addition, the formation, growth and movement of the vortex all occur in approximately 5 milliseconds. At M = 0.3, with the range of velocities encountered, the particles are subject to an acceleration of $O((10^3 - 10^4)m/s^2)$. It is clear that most particles may not be following the flow under these conditions. The small particles that may follow the flow would not scatter sufficient light to provide a good signal to noise ratio. The large dynamic range of the flow also reduces the SNR (as SNR is inversely proportional to bandwidth) It may be recalled here that in the present measurements, the system gains were optimized to get good signals over the whole cycle, that is, the gains were set intentionally some what low so that these measurements could be obtained. Hence low amplitude signals would not have been validated and thus, some of the signals from the backside of the vortex would

have been lost. The smallest velocity measured anywhere was about $0.15U_\infty$ as seen in histograms at some locations. These are largely responsible for the vortex not being seen in the measurements. Special seeding methods may mitigate this problem slightly, as also, conducting the experiment with large gains in the system with a method that validates the data below a preset amplitude limit so that only signals from small particles are indeed picked up and validated. Limiting the measurement to the phase angle range of interest would help too as in this method of measurement, a required number of samples will be obtained at each phase angle, rather than a total number in the whole cycle (This would also increase the experiment time enormously). The blockage of the beams by the airfoil will only add to these difficulties. All in all, the measurements are extremely difficult and some success has been achieved in the present study. Not seeing the dynamic stall vortex does not limit the usefulness of the data in anyway because the goal is to understand its formation and possible prevention. The 'game' is already 'lost' when the vortex begins to move.

5. Concluding Remarks

1. Velocity data over an oscillating airfoil in dynamic stall have been obtained for the first time. The velocity field exhibits interesting features over the entire domain of measurement.
2. The data show the formation of a separation bubble over the airfoil surface and its bursting just around where the dynamic stall vortex forms.
3. The velocity profiles over the airfoil change from that of a leading edge wall jet to a wake like distribution in an oscillation cycle depending upon the flow in the bubble.
4. The velocity field shows that the flow experiences rapid accelerations over a large region of the airfoil with values as high as $1.6U_\infty$ at a free stream Mach number of 0.3 and a reduced frequency of 0.05. Instantaneously, the velocities reached magnitudes of $1.8U_\infty$, but, no supersonic velocities were observed. It is believed that the formation of the bubble has modified the local pressure distribution sufficiently to grossly alter the flow.
5. The extent of the moving wall effect has been quantified and it is found to be much greater than previously assumed as flow accelerations can be seen at large distances (y/c = 0.5) from the airfoil.
6. Circulation (estimated from vorticity) was shown to increase monotonically until the dynamic stall vortex begins to convect.
7 The fact that the dynamic stall vortex was not found distinctly has been attributed to the limitations of the measurement technique and some possible methods of capturing it are offered. Further studies using the alternate methods of measurements discussed are expected to provide a more comprehensive information of the flow field

7

6. References

[1] Carr, L.W., "Progress in Analysis and Prediction of Dynamic Stall," *Jl. of Aircraft*, Vol. 25, No.1, Jan. 1988, pp. 6-17.

[2] McCroskey, W.J., "The Phenomenon of Dynamic Stall," NASA TM 81264, March 1981.

[3] Harper, P.W., and Flanigan, R.E., "The Effect of Change of Angle of Attack on the Maximum Lift of a Small Model," NACA TN 2061, March 1950.

[4] Chandrasekhara, M.S., and Carr, L.W., "Flow Visualization Studies of the Mach Number Effects on the Dynamic Stall of Oscillating Airfoils", *Jl. of Aircraft*, Vol. 27, No. 6, June 1990, pp. 516-522.

[5] Chandrasekhara, M.S., and Brydges, B.E., "Amplitude Effects on Dynamic Stall of an Oscillating Airfoil", *AIAA Paper No. 90-0575*, Jan. 1990.

[6] Chandrasekhara, M.S., Carr, L.W., and Ahmed, S., "Pitch Rate History Effects on Dynamic Stall", presented at the *NASA/AFOSR/ARO Workshop on Physics of Forced Unsteady Flow Separation*, April 1990.

[7] De Ruyck, J., Hazarika, B., and Hirsch, Ch., "Transition and Turbulence Structure in the Boundary Layers of an Oscillating Airfoil", *Final Technical Report*, VUB Report STR-16, Vrije Universiteit Brussel, Brussels.

[8] Grohsmeyer, S.P., Ekaterinaris, J.A., and Platzer, M.F., "Numerical Investigation of the Effect of Leading Edge Geometry on Dynamic Stall on Airfoils", *AIAA Paper No. 91-1798*, June 1991.

[9] Ekaterinaris, J.A., "Compressible Studies on Dynamic Stall", *AIAA Paper No. 89-0024*, Jan. 1989.

[10] Courier, J., and Fung, K.Y., "An Analysis of the Onset of Dynamic Stall", *AIAA Paper No. 91-0003*, Jan. 1991.

[11] Carr, L.W., and Chandrasekhara, M.S., "Design and Development of a Compressible Dynamic Stall Facility", *AIAA Paper No. 89-0647*, to appear in *Jl. of Aircraft*.

[12] Carr, L.W., Chandrasekhara, M.S., and Brock, N., "A Quantitative Visual Study of Unsteady Compressible Flow on an Oscillating Airfoil", *AIAA Paper No. 91-1683*, June 1991.

[13] Chandrasekhara, M.S., and VanDyken, R.D., "Oscillating Airfoil Velocity Field During Large Amplitude Dynamic Stall", *Proc. 8th Symposium on Turbulent Shear Flows*, Sep. 8-11, 1991, München, West Germany.

[14] Ericsson, L.E., "Moving Wall Effects in Unsteady Flow", *Jl. of Aircraft*, Vol. 25, No. 11, Nov. 1988, pp. 977-990.
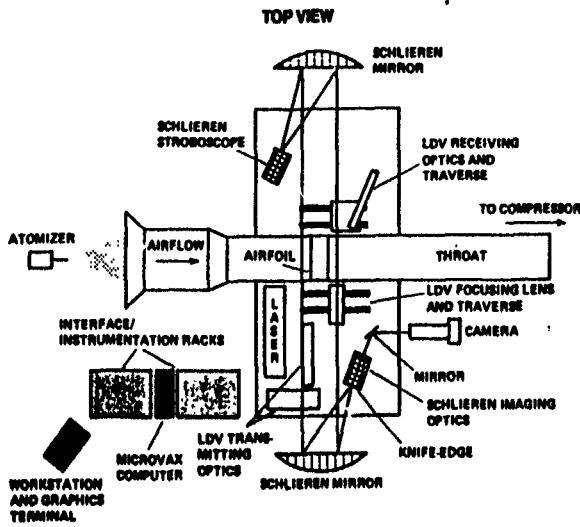
Fig. 1. Schematic of the CDSF Instrumentation.
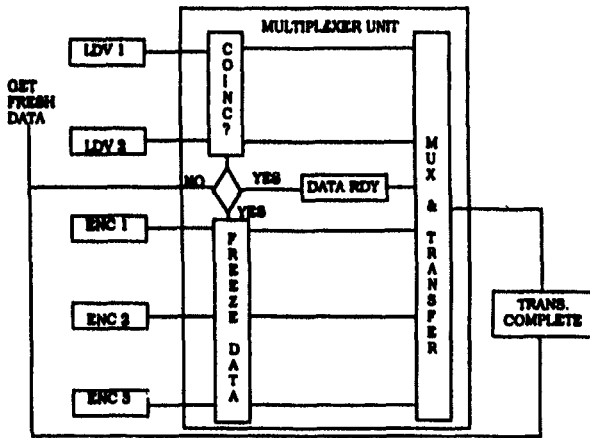
Fig. 2. Schematic of the LDV Data Acquisition Method.
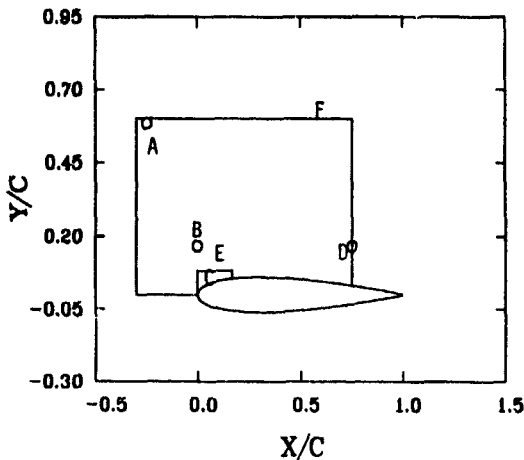
Fig. 3. Flow Domain for Discussion of Results.
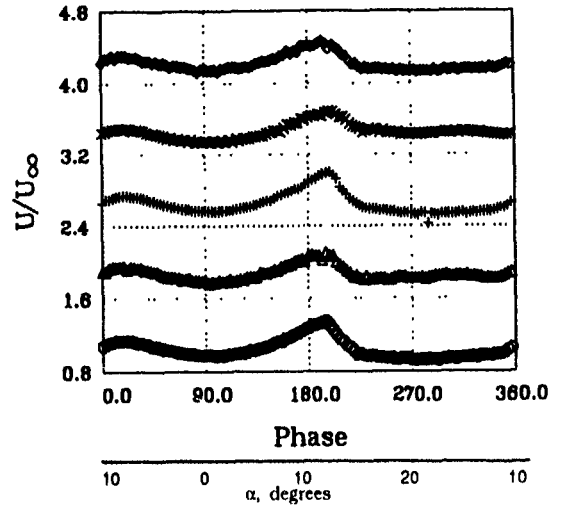
Fig. 4. Two Dimensionality Surveys: Normalized U Velocity Component, (Velocity Offset by $0.8\frac{U}{U_\infty}$), x/c = 0.0, y/c = 0.167.

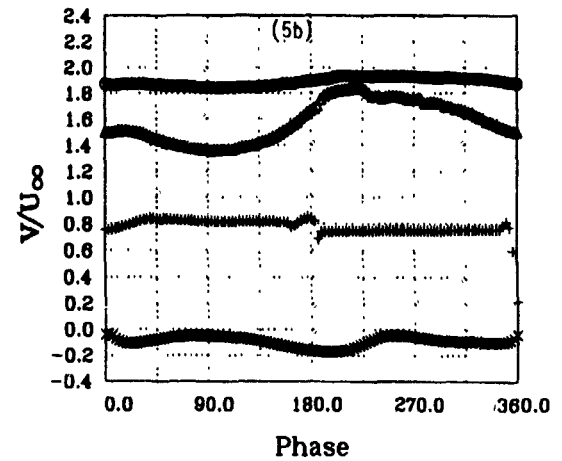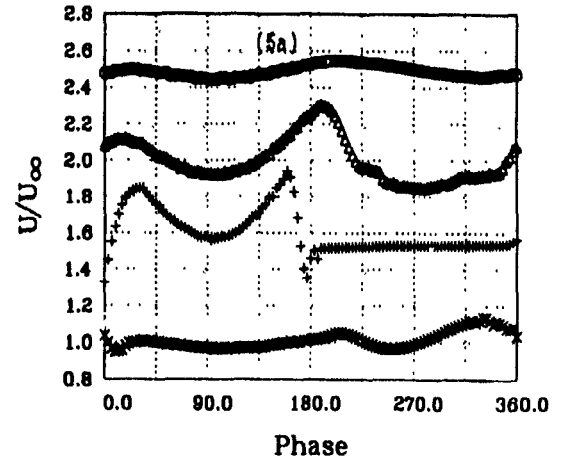o, z/c = -1.0; Δ, z/c = -0.5; +, z/c = 0.0; x, z/c = 0.5; $\diamond$, z/c = 0.833.

Fig. 5. Typical Velocity Distributions With Phase (a) U Component (Velocity Offset by $0.5\frac{U}{U_\infty}$), (b) V Component (Velocity Offset by $0.6\frac{U}{U_\infty}$)

o, x/c = -0.25, y/c = 0.583; Δ, x/c = 0 0, y/c = 0.117; +, x/c = 0.083, y/c = 0 067; x, x/c = 0 750, y/c = 0.133.

9
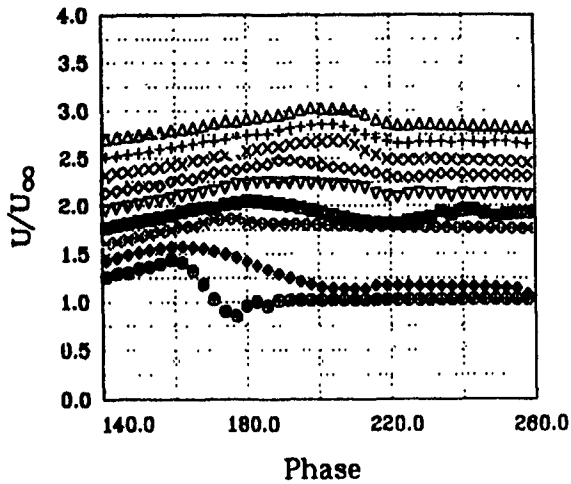
Fig. 6a.
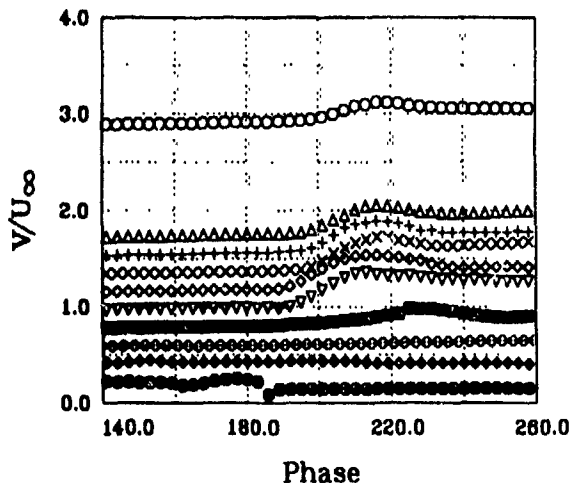
Fig. 6b.

Fig. 6. Measurements in the Separation Bubble: (a) U Component, (b) V Component, (Velocity Offset by $0.2\frac{U}{U_\infty}$), x/c = 0.083.

O	Y/C = 0.300		▽	Y/C = 0.133
△	Y/C = 0.200		⊞	Y/C = 0.117
+	Y/C = 0.183		✕	Y/C = 0.100
✕	Y/C = 0.167		◆	Y/C = 0.083
◇	Y/C = 0.150		⊞	Y/C = 0.067

|V| (offset)
Fig. 7a
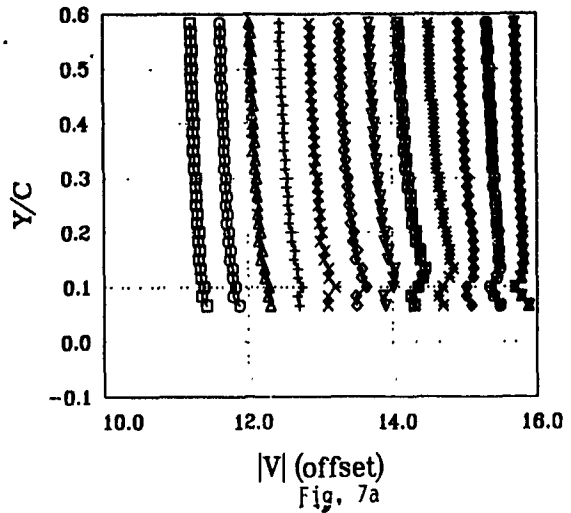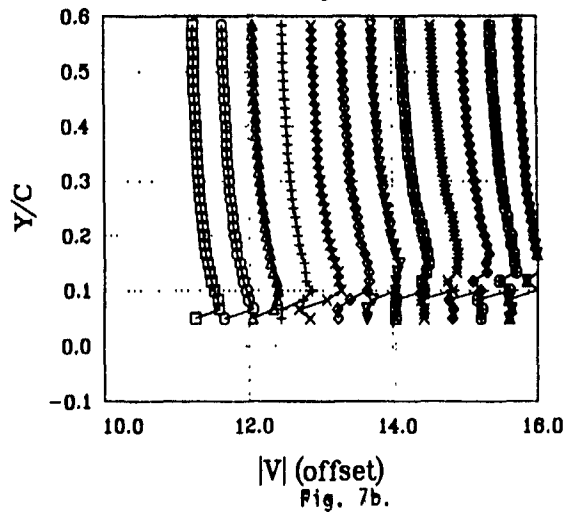
|V| (offset)
Fig. 7b.
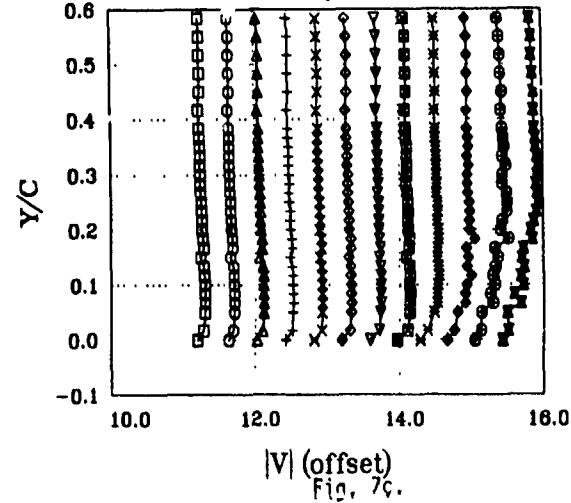
|V| (offset)
Fig. 7c.

Fig. 7. Absolute Velocity Distributions With Phase (Velocity Offset by $0.2\frac{U}{U_\infty}$ at Each Phase), (a) x/c = 0.0, (b) x/c = 0.083, (c) x/c = 0.583.

—☐—	ψ=153.0 ,SHIFT= 10 20		—▽—	ψ=189.0, SHIFT= 12.60
—⊖—	ψ=159.0, SHIFT= 10.60		—⊞—	ψ=195.0, SHIFT= 13.00
—△—	ψ=165 0, SHIFT= 11 00		—✕—	ψ=201 0, SHIFT= 13 40
—+—	ψ=171.0, SHIFT= 11.40		—◆—	ψ=207.0, SHIFT= 13.80
—✕—	ψ=177 0, SHIFT= 11.80		—⊕—	ψ=213.0, SHIFT= 14.20
—◆—	ψ=183 0, SHIFT= 12 20		—■—	ψ=219.0, SHIFT= 14 60
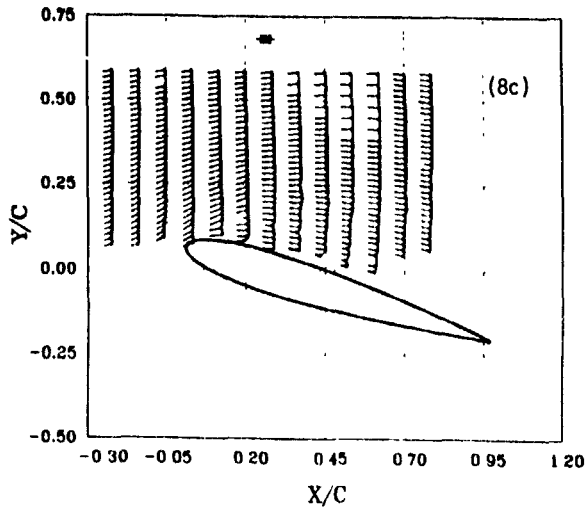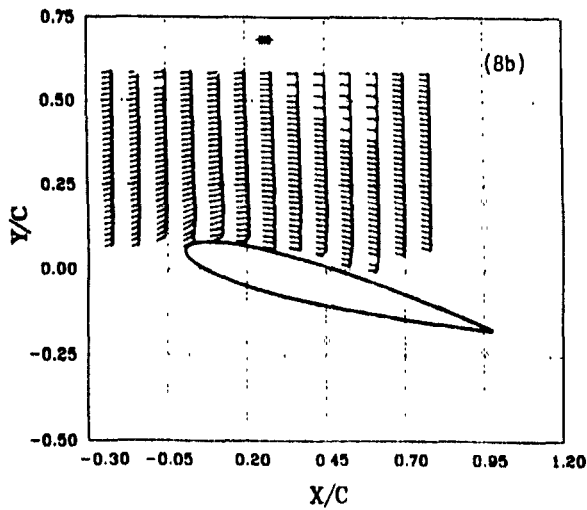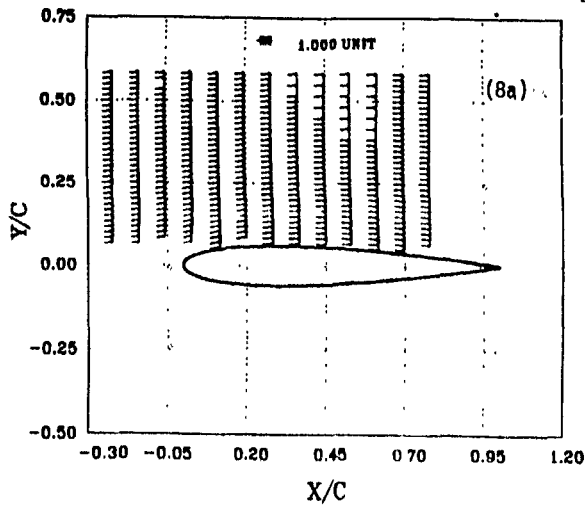
Fig 8 Absolute Velocity Distribution (a) $\phi = 90^0, \alpha = 0^0$, (b)$\phi = 201^0, \alpha = 13.6^0$, (c) $\phi = 216^0, \alpha = 15.9^0$.
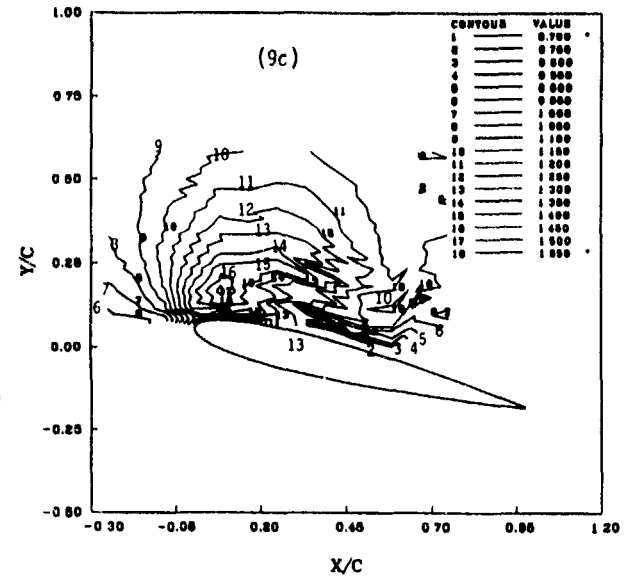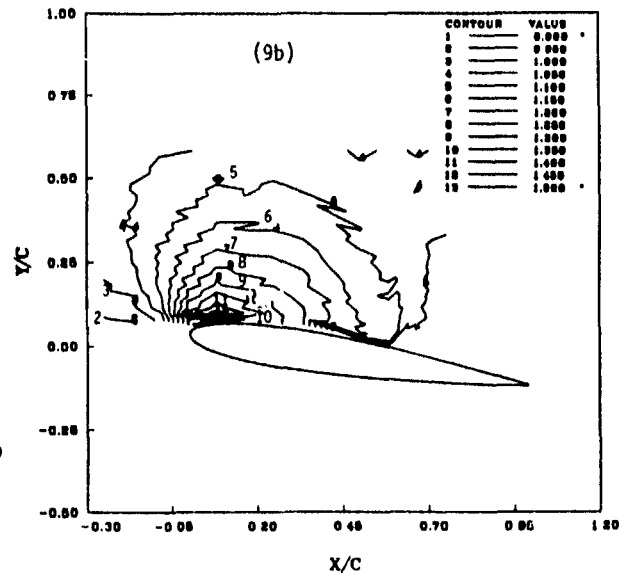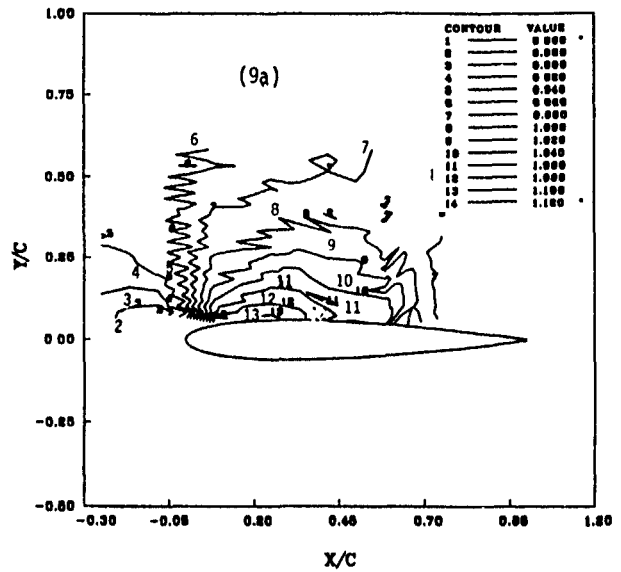

Fig 9 Contours of Absolute Velocity (a) $\varphi = 90^0, \alpha = 0^0$, (b)$\phi = 174^0, \alpha = 8.95^0$, (c) $\varphi = 204^0, \alpha = 14.07^0$ (Continued). *, No Contour Lines Found

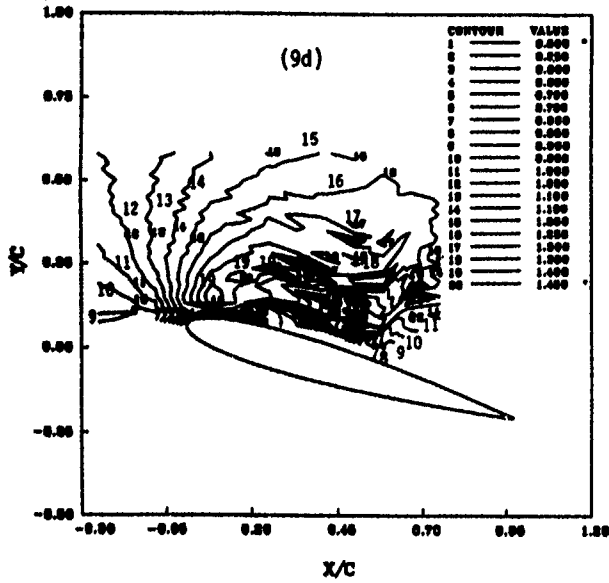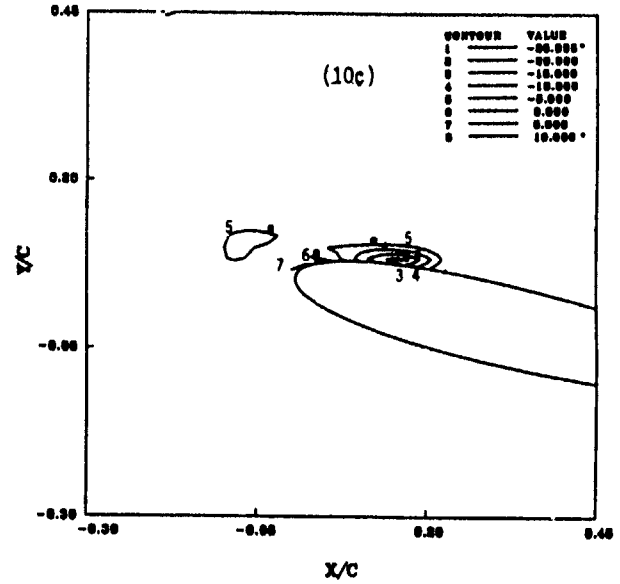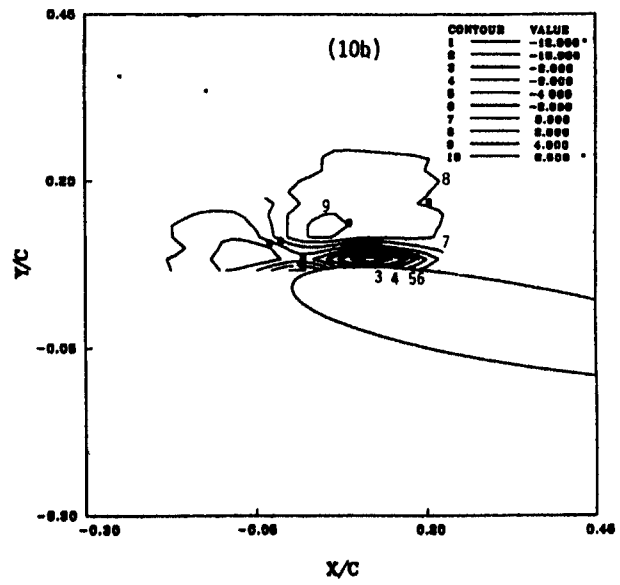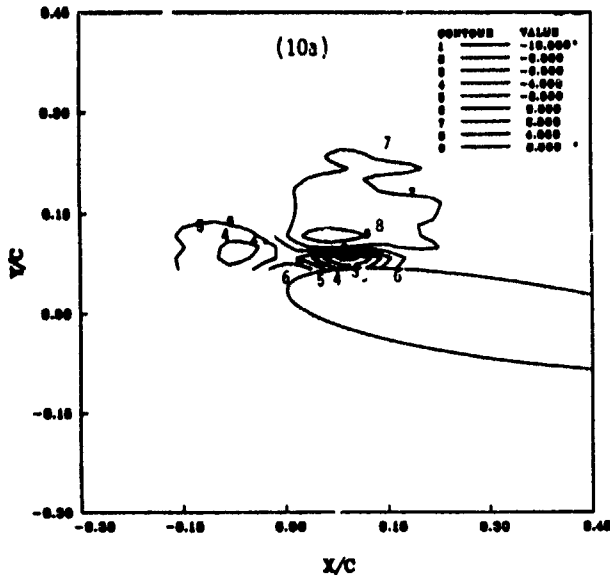Fig. 9 (d) $\phi = 216^0, \alpha = 15.9^0$, (Concluded).

Fig. 10. Contours of Normalized z-Component of Vorticity: (a) $\phi = 171^0, \alpha = 8.44^0$, (Continued), *, No Contour Lines Found.

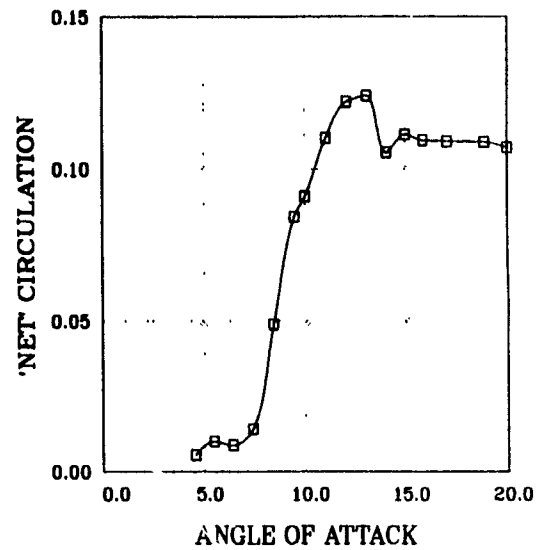Fig. 10. (b)$\phi = 180^0, \alpha = 10.0^0$, (c) $\phi = 198^0, \alpha = 13.09^0$, (concluded).

Fig. 11. Variation of Net Circulation' With Angle of Attack.

12